npj | Quantum Materials

www.nature.com/npjquantmats

ARTICLE OPEN

Check for updates

Berry curvature origin of the thickness-dependent anomalous Hall effect in a ferromagnetic Weyl semimetal

Yao Zhang[1,2,3,6], Yuefeng Yin[4,5,6], Guy Dubuis[1,2], Tane Butler[1], Nikhil V. Medhekar[4,5]✉ and Simon Granville[1,2]✉

Magnetic Weyl semimetals with spontaneously broken time-reversal symmetry exhibit a large intrinsic anomalous Hall effect originating from the Berry curvature. To employ this large Hall current for room temperature topo-spintronics applications, it is necessary to fabricate these materials as thin or ultrathin films. Here, we experimentally demonstrate that Weyl semimetal Co_2MnGa thin films (20–50 nm) show a large anomalous Hall angle ~11.4% at low temperature and ~9.7% at room temperature, which can be ascribed to the non-trivial topology of the band structure with large intrinsic Berry curvature. However, the anomalous Hall angle decreases significantly with thicknesses below 20 nm, which band structure calculations confirm is due to the reduction of the majority spin contribution to the Berry curvature. Our results suggest that Co_2MnGa is an excellent material to realize room temperature topo-spintronics applications; however, the significant thickness dependence of the Berry curvature has important implications for thin-film device design.

npj Quantum Materials (2021)6:17 ; https://doi.org/10.1038/s41535-021-00315-8

INTRODUCTION

In Weyl semimetals (WSMs), a type of topological semimetal, the valence and conduction bands touch each other at isolated points called Weyl nodes, which can be understood as the monopoles and anti-monopoles of Berry curvature in momentum space[1]. Chiral Weyl fermions, as low-energy quasiparticle excitations around these Weyl nodal points, can be pumped along surface Fermi arcs that connect the paired Weyl nodes. Due to this non-trivial topology of band structure, WSMs display a rich variety of exotic transport properties[2,3], like negative magnetoresistance, and giant magnitudes of anomalous Hall effect (AHE), planar Hall effect, and anomalous Nernst effect (ANE).

Magnetic WSMs additionally have spontaneously broken time-reversal symmetry, resulting in large intrinsic AHE originating from the Berry curvature[4–6]. The intrinsic AHE current is dissipationless and fully spin-polarized and therefore has great potential for spintronics applications[7]. There is suggestion that magnetic WSMs could allow for the quantum anomalous Hall effect to persist at high temperatures[8]. Recently, kagome-lattice compound $Co_3Sn_2S_2$ has been proven to be a magnetic WSM with giant anomalous Hall conductivity σ_{xy} ~1130 Ω^{-1} cm^{-1} and anomalous Hall angle, 20%[9], and thin films also exhibit the same transport behaviour as the bulk single crystal[10]. However, $Co_3Sn_2S_2$ shows a low Curie temperature $T_c = 177$ K, which means it cannot be used for room temperature devices. Co-based Heusler compounds, face-centered cubic metallic compounds with space-group symmetry $Fm\bar{3}m$(225), have been predicted to be promising candidates to realize magnetic WSMs with high Curie temperature[4,6]. Recent attention has also focused on magnetic Heusler alloys due to the wide tunability of the Berry curvature predicted in this materials class[2,11,12].

What's more, these materials are soft ferromagnets, meaning that the spin orientation can be easily manipulated by applying a small magnetic field. Recently, bulk examples of full Heusler ferromagnet Co_2MnGa with large Curie temperature $T_c \approx 700$ K have been studied and shown to display giant ANE and large anomalous Hall angle, 12%, at room temperature, due to a large net Berry curvature near the Fermi energy associated with nodal lines and Weyl points[10,13,14]. In addition, Tung et al.[15] and Manna et al.[12], by calculating the Hall conductivity contribution of the majority and minority spin channels from bulk Co_2MnGa, found the spin-up and spin-down Hall currents would flow in opposite directions and the large σ_{xy} results almost entirely from the majority spin channel. In this case, the anomalous Hall current would be nearly fully spin-polarized, even though Co_2MnGa is not a half-metallic ferromagnet. The combination of topological electronic properties, ferromagnetism above room temperature, and strongly spin-polarized anomalous Hall current make Co_2MnGa an exceptional candidate for studying the interplay of topology and magnetism and realizing room temperature topo-spintronics applications, such as magnetic field sensing[16] and generating spin-transfer torque[17].

To realize these applications, Co_2MnGa needs to be fabricated as thin films. There are studies of thin films prepared by molecular beam epitaxy[18–20], flash evaporation[21], or magnetron sputtering[22–24]; however, almost all of this work was done before the topological characteristics of this material were realised. Hence, there has so far been very little research about the transport properties related to the topological band structure in Co_2MnGa thin films. Reichlova et al. found that Co_2MnGa thin films exhibit a large ANE coefficient at 300 K, −2 to −3 μV K^{-1}, due to the non-trivial band structure[24,25]. However, this coefficient decreases significantly with thickness down to 10 nm and the reason still needs to be uncovered. Very recently, Markou and Wang et al. investigated thick Co_2MnGa thin films, which show the same value of anomalous Hall angle as in the single crystals[26,27], but they did not address the reason for the decline of anomalous Hall angle with decreasing

[1]Robinson Research Institute, Victoria University of Wellington, Wellington, New Zealand. [2]MacDiarmid Institute for Advanced Materials and Nanotechnology, Wellington, New Zealand. [3]School of Chemical and Physical Sciences, Victoria University of Wellington, Wellington, New Zealand. [4]Department of Materials Science Engineering, Monash University, Clayton, MEL, Australia. [5]ARC Centre of Excellence in Future Low Energy Electronics, Monash University, Clayton, MEL, Australia. [6]These authors contributed equally: Yao Zhang, Yuefeng Yin. ✉email: nikhil.medhekar@monash.edu; Simon.Granville@vuw.ac.nz

thickness. Investigating the properties of ultrathin films is important for understanding the prospect of producing energy-efficient, high-density spintronic devices, as well as investigating the potential effects of their low dimensionality on the Berry curvature. In previous work we showed that ultrathin (>3.5 nm) films of polycrystalline Co_2MnGa display perpendicular magnetic anisotropy (PMA) in trilayer MgO/Co_2MnGa/Pd stacks[28], which could be used to reduce the switching current in spin-transfer torque devices[29].

For a comprehensive understanding of Weyl topological effects on the AHE in magnetic WSM thin films, we systematically investigated the transport properties of Co_2MnGa thin films with thicknesses from 50 nm down to 5 nm. The thicker films exhibit a large anomalous Hall angle in agreement with the recent results of Markou et al., and ascribed to the intrinsic Berry curvature as found from calculations of bulk Co_2MnGa. However, for films thinner than 15 nm, the anomalous Hall angle drops significantly due to the reduction of the majority spin contribution to the Berry curvature, proving that tuning the Berry curvature can be achieved in this Heusler alloy and opening possibilities for engineering topo-spintronic materials and devices.

RESULTS

Crystal structure

For the 50-nm film, the θ–2θ scan of XRD shows the substrate MgO(002) peak and also Co2MnGa(002) and (004) peaks, as shown in Fig. 1a, indicating a good out of plane texture. Other MgO[00 *l*] lines are indicated by an asterisk, *. The inset is the rocking curve from the (004) peak, and the full width at half maximum (FWHM) is 0.779° suggesting a high crystal quality. Furthermore, the X-ray φ scans from −45° to 315° (Fig. 1b) display a fourfold symmetry of the Co_2MnGa(220) peak and the 45° rotation of these peaks relative to the substrate (220) peaks, confirming the epitaxial relationship of MgO(001)[100]||Co_2MnGa(001)[110]. We also obtained the superstructure (111) peak with in-plane XRD, which shows fourfold symmetry in the φ scan as well, as shown in the top panel of Fig. 1b. In full Heusler alloys, the XRD peaks with all odd (*hkl*) indexes, like (111), are known to originate in superlattice reflections in the $L2_1$ structure[30]. The in-plane *a*–*b* and *c*-axis lattice constants are 5.765 Å and 5.759 Å ($c/a = 0.999$), respectively, obtained from the (004) and (111) peaks. The strain $\varepsilon = (a_{||} - a_0)/a_0$ is estimated as −0.035%, where a_0 is the lattice constant of bulk single crystal Co_2MnGa (5.767 Å)[31] and $a_{||}$ is the in-plane lattice constant of thin film (5.765 Å). Even though the diagonal $\sqrt{2}a_{MgO}$ of the substrate is 5.962 Å, which could induce a 3.27% lattice mismatch, the stress in our thin film is almost fully relaxed due to the post-annealing at 550 °C for 1 h. The film roughnesses measured by XRR or AFM are below 1 nm, as shown by example for the 20-nm thick film in Fig. 1c. Fitting the XRR results in a root-mean-square roughness (R_q) of 0.7 nm, with the thickness 20 nm ±2 nm. The AFM image confirms a smooth surface morphology with a R_q of 0.5 nm, as shown in the insert of Fig. 1c.

Magnetotransport properties

Magnetic hysteresis loops of a 50-nm Co_2MnGa film were measured with the external magnetic field along both the in-plane and out-of-plane directions at 300 K, as shown in Fig. 2a. These show the easy axis is along the Co_2MnGa[110] direction, the same as for other Heusler alloy thin films, Co_2MnAl Co_2MnSi[32,33], and the coercive field $\mu_0 H_c$ and saturation magnetization M_s are 3 mT, 600 emu cm^{-3}, respectively. Note that the crystalline direction used in this paper refers to the Co_2MnGa lattice, unless indicated otherwise. When the magnetic field is along the [100] direction, though it shows a small coercive field $\mu_0 H_c = 1$ mT, the saturation field is 25 mT, larger than along the [110] direction. For the [001] direction, the saturation field is 1 T (see Supplementary Fig. 1), but it still shows a small square loop, interestingly indicating there is a

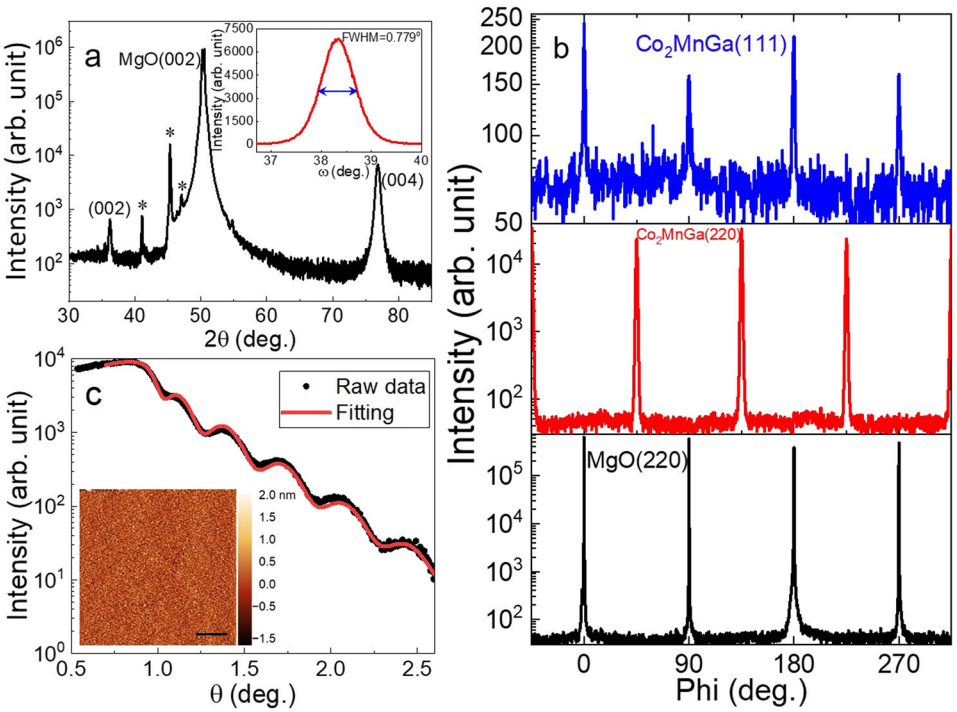

Fig. 1 Crystal structure and surface morphology of Co_2MnGa. a θ–2θ scan, the inset is the rocking curve from (004) peak, and **b** in-plane φ scans from −45° to 315°, for 50 nm Co_2MnGa thin films. **c** X-ray reflectivity for the 20 nm Co_2MnGa thin film, the inset is the atomic force microscopy image (5 × 5 μm^2) with colour contrast (dark to bright) for the height scale corresponds to 3.5 nm. The scale bar corresponds to 1 μm.

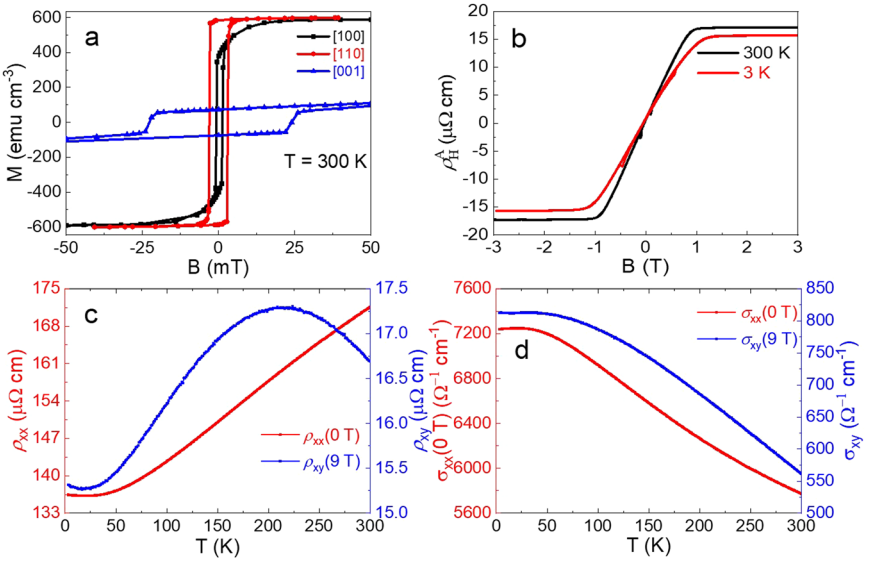

Fig. 2 Magnetic and electric transport measurements for 50 nm Co_2MnGa. a Magnetization measured at 300 K with the magnetic field along in-plane and out-of-plane direction, respectively. **b** Anomalous Hall effect measurements at 3 and 300 K, respectively. **c** Longitudinal resistivity without field (red) and Hall resistivity cooling down with 9 T (blue) as a function of temperature from 3 to 300 K. **d** the corresponding conductivity as a function of temperature from 3 to 300 K.

small out-of-plane magnetization component at zero applied field. The uniaxial anisotropy energy density calculated from the hard [001] and easy [110] directions is 3.05×10^6 erg cm^{-3}. The Hall resistivity as a function of magnetic field was measured at 300 K and 3 K, respectively, as shown in Fig. 2b. For all of our samples, the current was applied along the [100] direction. The pure anomalous Hall resistivity was calculated by using $\rho_H^A = \rho_{xy} - R_o B_z$, where R_o is the ordinary Hall coefficient and B_z is the magnetic flux density along out-of-plane direction. The Hall coefficient R_o is negative and quite small, -2.42×10^{-4} cm^3 C^{-1} (300 K) and -1.06×10^{-4} cm^3 C^{-1} (3 K), meaning that charge carriers are of the electron type. The anomalous Hall saturation fields at 300 and 3 K are 1.3 and 1.6 T, respectively. The anomalous Hall resistivities are 17.1 and 15.4 μΩ cm at 300 and 3 K, respectively, and the ordinary Hall resistivities at 9 T are 0.218 μΩ cm (300 K) and 0.095 μΩ cm (3 K). The Hall carrier concentration and Hall mobility are 2.58×10^{22} cm^{-3} and 1.41 cm^2 V^{-1} s^{-1}, respectively, at 300 K. Since the ordinary Hall resistivity is negligible in our samples, it is safe to adopt ρ_{xy} as nearly equal to the anomalous Hall resistivity. The knot in the resistivity curve also indicates the out-of-plane magnetization component seen in the magnetization measurements. In Fig. 2c, the temperature dependence of Hall resistivity ρ_{xy} and longitudinal resistivity ρ_{xx} obtained from 300 to 3 K are plotted. The 50-nm Co_2MnGa thin film has a residual resistivity $\rho_o = 136$ μΩ cm at 23 K and exhibits a typical metallic behaviour at higher temperature (red curve). The ρ_{xy}increases with T, displaying a maximum value 17 μΩ cm around 210 K, followed by a decrease to higher temperature (blue curve). The Curie temperature of Co_2MnGa is much higher than room temperature (see Supplementary Fig. 2), and consistent with the bulk T_c ~700 K[34]. The Hall conductivity σ_{xy} and longitudinal conductivity σ_{xx} were calculated by using $\sigma_{xy} = \rho_{xy}/(\rho_{xy}^2 + \rho_{xx}^2(0T))$ and $\sigma_{xx} = \rho_{xx}/(\rho_{xy}^2 + \rho_{xx}^2(0T))$, respectively. Both Hall conductivity (blue curve) and longitudinal conductivity (red curve) increase monotonically on cooling and approach constant values of 812 and 7250 Ω^{-1} cm^{-1}, respectively, at low temperature, as shown in Fig. 2d.

The anomalous Hall angle can be calculated by using $\theta_H = \sigma_{xy}/\sigma_{xx}$. Figure 3a shows the anomalous Hall angle as a function of temperature from 300 to 3 K. The 50-nm topological semimetal Co_2MnGa thin film shows a large anomalous Hall angle $\theta_H = 9.7\%$ at 300 K, increasing at low temperature to reach a maximum value 11.4% at 113 K. Usually, typical ferromagnetic thin films with topologically trivial band structure show a small angle, less than 3%[35]. Even though some non-magnetic Weyl semimetals exhibit giant anomalous Hall angle in single crystals[36,37], to date only Co_2MnGa shows such a large anomalous Hall angle in thin films at room temperature.

In non-magnetic WSMs, the existence of planar Hall effects or negative magnetoresistances has also been taken as further evidence of the effect of the Weyl character of the band structure on the electronic transport[38,39]. However, both of these effects are present in magnetic non-Weyl materials also, and the measurements of these effects in magnetic WSM $Co_3Sn_2S_2$ are unremarkable and consistent with a trivial magnetic origin[40]. In Supplementary Figs. 4 and 5 we show the angle-dependent planar Hall effect and magnetoresistance of our films measured along several crystallographic directions. The magnitudes of these effects are similar to those measured in $Co_3Sn_2S_2$[9,40] and are not larger than in typical magnetic non-Weyl materials. What's more, the linear negative MR observed at high field in Co_2MnGa when the magnetic field is parallel to the current, as shown in Supplementary Fig. 5, can be ascribed to the thermal-induced spin disorder, which is a typical ferromagnet behaviour[41,42]. Therefore, we consider the large anomalous Hall angle to be the only consistent magnetotransport indicator of the topological non-trivial band structure in ferromagnetic WSMs such as Co_2MnGa.

To understand the thickness dependence of the anomalous Hall angle, we fabricated Co_2MnGa films with smaller thicknesses, from 20 to 5 nm. Supplementary Fig. 3 shows the ρ_{xx} and ρ_{xy} as a function of temperature from 3 to 300 K for Co_2MnGa (5–50 nm). Figure 3b shows the thickness dependence of the anomalous Hall angle measured from 300 to 3 K. Once we decrease the thickness to 20 nm, the anomalous Hall angle is still large, around 11%, and this film shows a similar trend as the 50-nm film when decreasing the temperature. However, for samples with thicknesses of 15, 10, and 5 nm, the anomalous Hall angle is temperature independent, and the value drops to 3.3%, 2.7%, and 1.3%, respectively. The inset

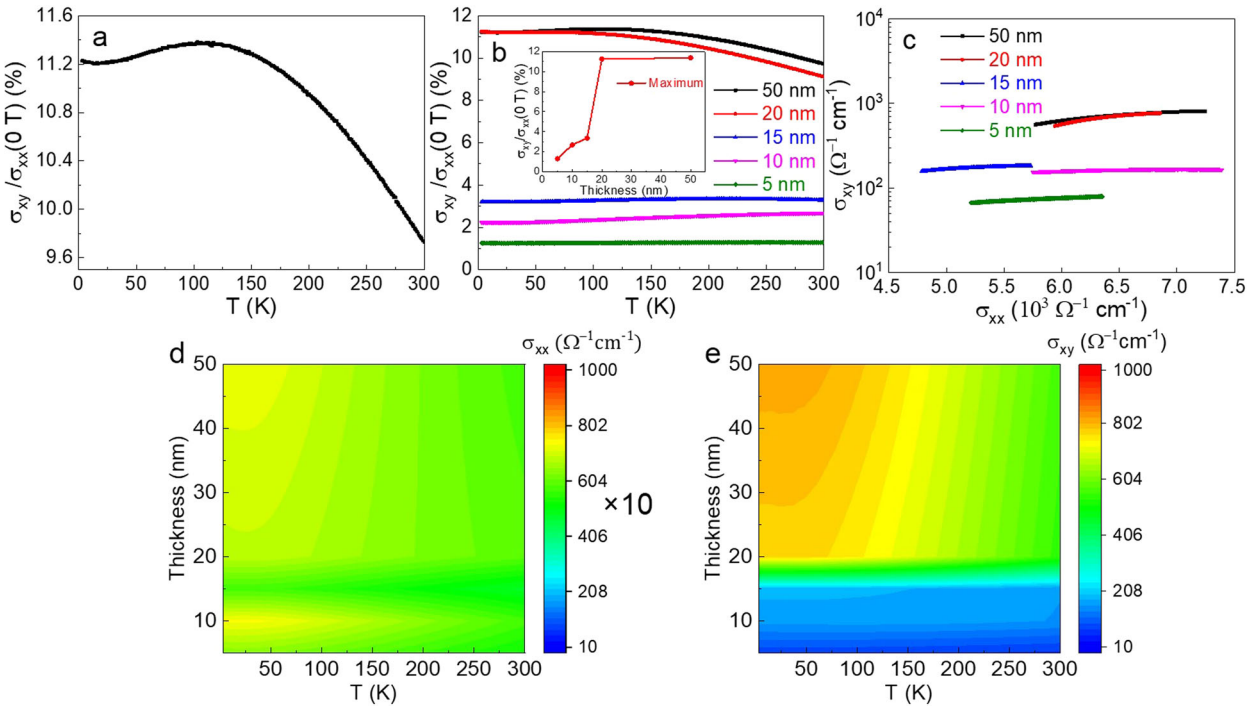

Fig. 3 Transport measurement of the anomalous Hall angle. a Temperature dependent anomalous Hall angle measured from 3 to 300 K for 50 nm Co_2MnGa. **b** Thickness dependence of anomalous Hall angle as a function of temperature from 3 to 300 K, the inset is the maximum anomalous Hall angle as a function of thickness. **c** Log σ_{xy} - σ_{xx} plot for Co_2MnGa with thicknesses from 5 to 50 nm. **d**, **e** Thickness dependence of σ_{xx} and σ_{xy} as a function of temperature from 3 to 300 K, respectively.

shows the maximum value of each sample, as measured between 3 and 300 K. Our results of thinner samples agree very well with ref. [42] in which the anomalous Hall angle of 6 nm Co_2MnGa is no more than ~2.8%. Figure 3c is the log σ_{xy} - σ_{xx} plot for all samples measured at 300 to 3 K. σ_{xx} is about 4.5–7.5 $\times 10^3\ \Omega^{-1}\ cm^{-1}$ at various thicknesses and temperatures, and σ_{xy} is nearly independent of σ_{xx}. For the samples with thicknesses from 50 to 20 nm, one can see that σ_{xy} is nearly constant (around $700\ \Omega^{-1}\ cm^{-1}$). It is known that there exist three regimes in the scaling behaviour of the AHE depending on the range of σ_{xx}, categorized by a scaling parameter, a, in $\sigma_{xy} \propto \sigma_{xx}^{a}$ [43]. The values of σ_{xx} of all samples are close to the intermediate region as defined in ref. [43], where $\sigma_{xx} = 10^4$–$106\ \Omega^{-1}\ cm^{-1}$. Furthermore, this constant value of σ_{xy} is close to the order of the intrinsic contribution. This is the value expected from the intrinsic scattering-independent mechanism originating from the Berry curvature in momentum space, and indicates that σ_{xy} in our films is dominated by the intrinsic component due to the non-trivial topology of band structure of Co_2MnGa[35]. However, for the thinner samples with thicknesses of 15, 10, and 5 nm, the values of σ_{xy} drop steeply to 170, 160, and $70\ \Omega^{-1}\ cm^{-1}$, respectively. Since the values of σ_{xy} of these samples are much smaller than the order of the intrinsic contribution, the σ_{xy} might be due not only to the intrinsic scattering, but also might include contributions from the extrinsic side-jump mechanism, which can also induce values of σ_{xy} that are independent of σ_{xy}[44]. This agrees with our previous results that the σ_{xy} of polycrystalline MgO/Co_2MnGa/Pd ultrathin films results from both intrinsic and side-jump scattering[28]. Figure 3d and e show the σ_{xx} and σ_{xy} against the temperature and thickness, respectively. The σ_{xx} slightly increases with decreasing temperature, and then remains constant at low temperature. σ_{xx} for all samples at various temperatures varies only by ~25%; however, the σ_{xy} drops suddenly once the thickness is below 15 nm. For instance, comparing the 50 nm and 10 nm films, the σ_{xx} of both is around $7.2 \times 10^3\ \Omega^{-1}\ cm^{-1}$ at 3 K, but the σ_{xy} drops from 810 to $160\ \Omega^{-1}\ cm^{-1}$ for the thinner film.

Evolution of Berry curvature and surface band structure

The intrinsic contribution to the σ_{xy} is dependent only on the band structure of a material. It can be calculated from the Kubo formula for the Hall conductivity

$$\sigma_{xy} = \frac{e^2}{\hbar}\int \frac{d\boldsymbol{k}}{2\pi^3} f(\varepsilon_k)\Omega_z, \tag{1}$$

where $f(\varepsilon_k)$ is the Fermi-Dirac distribution function, Ω_z is the z-component Berry curvature[45]. The σ_{xy} can also be found from the sum of the conductivities for majority spin electrons (↑) and minority spin electrons (↓), $\sigma_{xy} = \sigma_{xy}^{\uparrow} + \sigma_{xy}^{\downarrow}$. Thus, the spin polarization-dependent conductivities $\sigma_{xy}^{\uparrow}$ and $\sigma_{xy}^{\downarrow}$ can be calculated by taking the integral of $\Omega_z^{\uparrow}$ and $\Omega_z^{\downarrow}$ over the entire Brillouin zone (BZ). Manna et al., by calculating the Hall conductivity contribution of the majority and minority spin channels from bulk Co_2MnGa, found σ_{xy} ~$1600\ \Omega^{-1}\ cm^{-1}$ and $\sigma_{xy}^{\downarrow}$ is almost equal to 0 at the Fermi level (E_F)[12]. The value of σ_{xy} in our thin films is half that of bulk Co_2MnGa. However, interestingly we have almost the same anomalous Hall angle of the bulk reports, 12%, since the value of σ_{xx} in our thin film is relatively smaller than in ref. [12].

To understand the influence of spin-dependent electrons for σ_{xy} of Co_2MnGa thin films with different thickness, we calculate the averaged z-component of the Berry curvature (total Berry curvature/number of slabs) and surface band structure from majority spin electrons and minority spin electrons near the Fermi level in the $k_x - k_y$ plane, respectively, as shown in Fig. 4 and Supplementary Fig. 6. For 123 primitive cell (50.1 nm) thick slab of Co_2MnGa, $\Omega_z^{\uparrow} \gg \Omega_z^{\downarrow}$ (see Fig. 4b, d), meaning $\sigma_{xy}^{\uparrow} \gg \sigma_{xy}^{\downarrow}$ and suggesting that the Berry curvature contribution to σ_{xy} from the

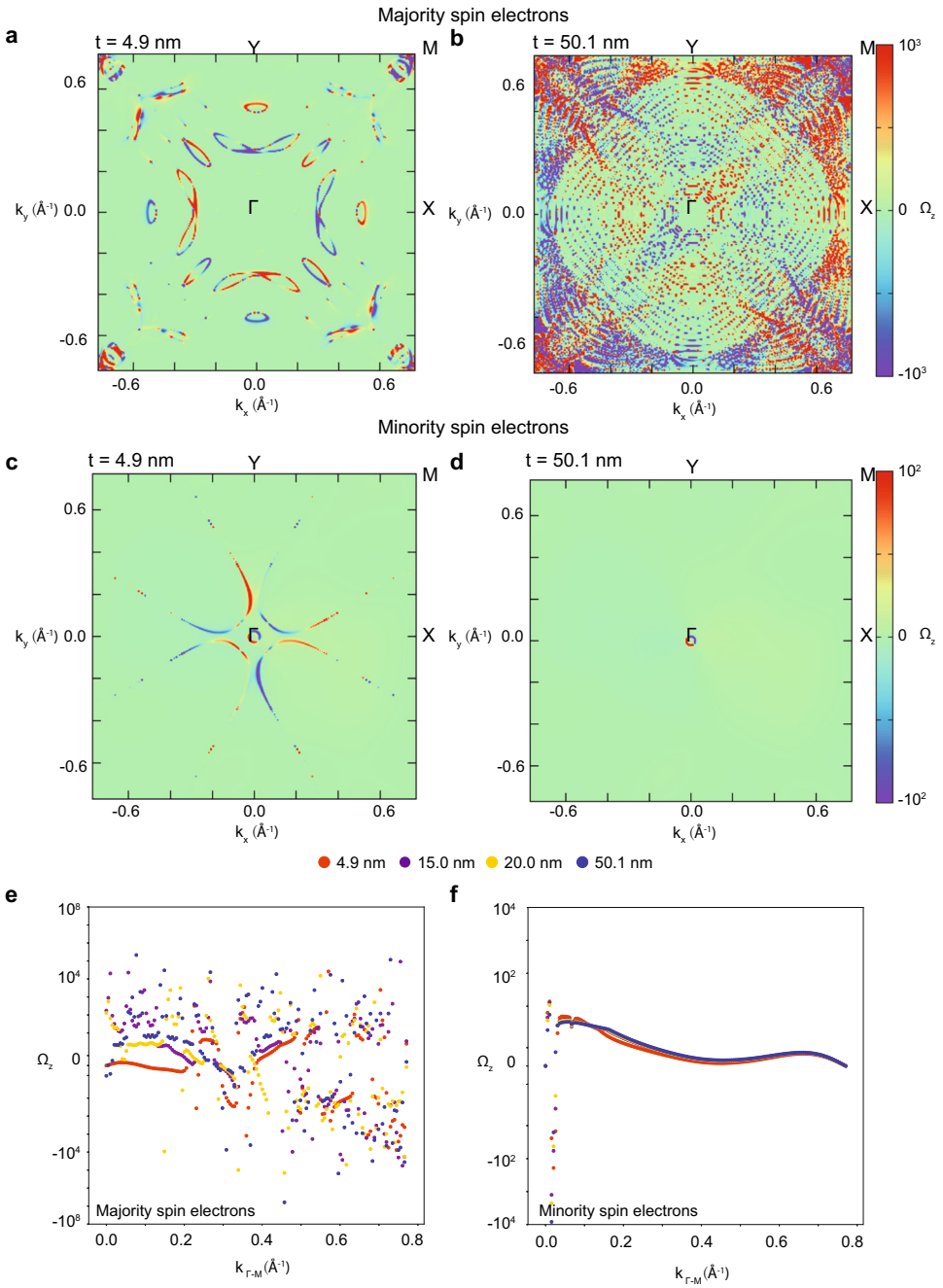

Fig. 4 Evolution of Berry curvature in Co_2MnGa thin films. a–d show the calculated averaged-integral of z-component Berry curvature (Ω_z) of occupied bands from minority and majority spin electrons for Co_2MnGa thin films of 4.9 nm and 50.1 nm, **e, f** show a comparison of Ω_z along Γ-M line for Co_2MnGa thin films of 4.9, 15.0, 20.0, and 50.1 nm.

majority spin electrons is much higher than that from minority spin electrons, which is the same as for bulk Co_2MnGa. Recent work has confirmed this by spin-resolved angle-resolved photoelectron spectroscopy on a 50-nm Co_2MnGa thin film[46]. The magnitude of $\Omega_z^{\uparrow}$ of this thick Co_2MnGa film is close to bulk values and is consistent with the σ_{xy} values calculated by others[10,12,15], suggesting films of ~50-nm thickness still show the bulk-like properties, like the large σ_{xy} originating from the non-trivial topology of the band structure with large intrinsic Berry curvature. The $\Omega_z^{\uparrow}$ for the 50-nm film in Fig. 4 is complicated because it includes multiple 'slabs' in the calculation, and at 50 nm there is not yet enough overlap of the states so that continuous bulk-like bands are formed. Once we decrease the thickness to 4.9 nm (12 primitive cells), $\Omega_z^{\uparrow}$ drops significantly (see Fig. 4b, d). This agrees with the experimental observation that the σ_{xy} reduces when film thickness decreases. Figure 4e and f summarises the $\Omega_z^{\uparrow}$ and $\Omega_z^{\downarrow}$ as a function of **k** along the Γ-M line for various thicknesses. The extent of Berry curvature reduction for majority spins is more significant than that for minority spins. Once the thickness is down to 20 nm, the $\Omega_z^{\uparrow}$ slightly drops, but it is still close to the bulk value indicating that the σ_{xy} is robust down to this thickness. Below 15 nm, the role of the surface becomes more important, which could result in extrinsic side-jump scattering and might suppress the effect of the Weyl nodes on the magnetotransport. What's more, there is a 3.27% lattice mismatch between Co_2MnGa and the MgO substrate. Though the stress in the 50-nm film is almost

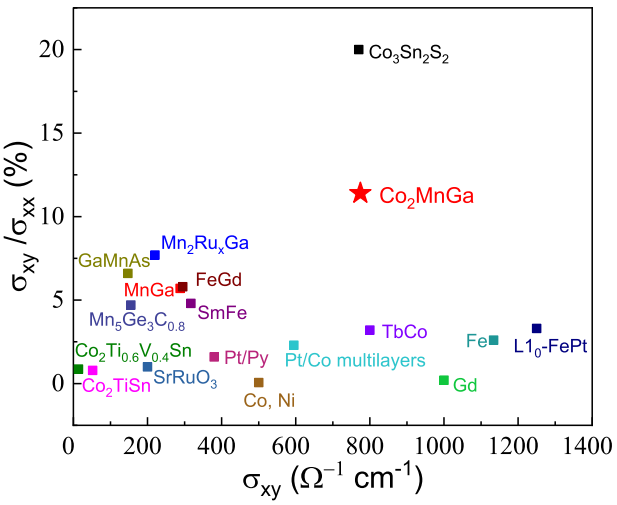

Fig. 5 The σ_{xy}-dependent anomalous Hall angle of our result in comparison with previously reported results for other thin films. The reported results were taken or calculated from references (see Supplementary Table 1).

fully relaxed due to the post-annealing, there could be a tetragonal distortion at low thickness which might induce an energy shift of the Weyl nodes[47] or shift the electron density-of-states[48]. Note the very different maxima used in the scales of Fig. 4a–d vs Fig. 4e–f, so that the main features can be seen in Fig. 4a–d, and the very large spikes can be seen in Fig. 4e–f.

DISCUSSION

By comparing to previously reported results of thin films, including Heusler alloys and classic ferromagnetic transition metal and alloys, the anomalous Hall angle in Co_2MnGa shows a large value, 11.4%, and also a comparatively large Hall conductivity 775 Ω^{-1} cm^{-1}, as shown in Fig. 5. To obtain a large anomalous Hall angle, the σ_{xy} needs to be large, or σ_{xx} needs to be small, but large σ_{xy} signal with very good signal-to-noise ratio is necessary for logic or memory hybrid CMOS/AHE devices[49] and AHE sensors[50]. Near the dirty regime[45] with a small σ_{xx}, however, σ_{xy} is suppressed more drastically than σ_{xx}, due to quasiparticle damping or spoiling of the resonance condition[51]. For ferromagnetic systems, both σ_{xy} and σ_{xy} are either large or small, and therefore the anomalous Hall angle is usually not very large. Though $Co_3Sn_2S_2$ thin films have a giant anomalous Hall angle 20%, it shows a low Curie temperature $T_c = 177$ K as we mentioned before. Even for exceptions such as the compensated Heusler ferrimagnet $Mn_{2-x}Ru_xGa$, which has a large anomalous Hall angle 7.7% at 300 K, it displays a small σ_{xy}, around 220 Ω^{-1} cm^{-1} [52].

In summary, we have prepared high quality epitaxial films of the topological semimetal Co_2MnGa with thicknesses from 5 to 50 nm on MgO substrates and established they have a similar large anomalous Hall angle at room temperature as in bulk crystals. For the 50-nm thick film, it shows large σ_{xy} ~775 Ω^{-1} cm^{-1} and anomalous Hall angle 11.4% at 113 K. The origin of the large σ_{xy} is the large net Berry curvature near the E_F due to the non-trivial topology of band structure of Co_2MnGa, and still shows a large anomalous Hall angle 9.7% at 300 K. The bulk-like properties are robust, for film thicknesses down to 20 nm. Once we decrease thickness below 20 nm, the σ_{xy} suddenly drops a lot with a slight change of σ_{xx}, with a corresponding decrease in the anomalous Hall angle. From our band structure calculations, we ascribe the decrease to the reduction of the majority spin electron Berry curvature. Our results confirm that Co_2MnGa is a topological magnetic material in which tuning of the Berry curvature is possible, as observed in the anomalous Hall behaviour. The opportunity to control the Berry curvature in materials provides a way to realize topo-spintronic logic or memory devices and AHE sensors that operate at room temperature.

METHODS

Sample preparation

Co_2MnGa (5–50 nm) thin films were epitaxially deposited on single-crystalline MgO(001) substrates in a Kurt J Lesker CMS-18 magnetron sputtering system with a base pressure below 5×10^{-8} Torr. Before fabricating thin films, substrates were cleaned with an Ar plasma, and then annealed at 400 °C for 1 h in the vacuum chamber. Co_2MnGa thin films were DC magnetron sputtered from a stoichiometric polycrystalline target at 100 W under 6 mTorr of Ar with a growth rate of 0.8 Å s^{-1} at 400 °C while rotating the sample holder. All samples were post-annealed in situ at 550 °C for 1 h to improve the lattice structure and the atomic ordering among Co, Mn, and Ga sites. After cooling down to ambient temperature, a 2-nm protective MgO layer was deposited on the top. Samples were patterned into standard Hall bars ($l = 2000$ μm, $w = 150$ μm) by photolithography and then Ar ion milling for magnetotransport characterization.

Thin-film characterization

The crystalline structure of the Co_2MnGa thin films was characterized by X-ray diffraction (XRD) with Co K_α radiation ($\lambda = 1.7889$ Å) using a Bruker D8 Advance. The film thicknesses were checked by X-ray reflectivity (XRR) using a PANalytical X'Pert PRO. Atomic force microscopy (AFM) was carried out on a Nanosurf FlexAFM mounted on a Nanosurf Isostage active vibration cancellation stand.

Magnetization and electric transport measurements

Magnetization measurements were performed using the RSO module of a Superconducting Quantum Interference Device magnetometer (SQUID, Quantum Design). The transport measurements were performed using the resistivity option of a Physical Property Measurement System (PPMS, Quantum Design).

Band structure calculation method

We used density functional theory (DFT) calculations as implemented in the Vienna ab initio Simulation Package (VASP) to calculate the optimized geometry and the electronic structure of Co_2MnGa[53]. The Perdew-Burke-Ernzehof (PBE) form of the generalized gradient approximation (GGA) was used to describe electron exchange and correlation[54]. The kinetic energy cut-off for the plane-wave basis was set to 400 eV. We used a $12 \times 12 \times 12$ Γ-centered **k**-point mesh for sampling the Brillouin zone. For calculation of Berry curvature of Co_2MnGa thin films, we adopted the method as implemented in the open-source code WannierTools[55,56], based on the Wannier tight-binding Hamiltonian obtained from wannier90[57]. Co/Mn *d* and Ga *s*, *p* orbitals are projectors for tight-binding Hamiltonian construction.

DATA AVAILABILITY

The data that support the findings of this study are available from the corresponding authors upon reasonable request.

Received: 16 September 2020; Accepted: 19 January 2021;
Published online: 19 February 2021

REFERENCES

1. Armitage, N. P., Mele, E. J. & Vishwanath, A. Weyl and Dirac semimetals in three-dimensional solids. *Rev. Mod. Phys.* **90**, 015001 (2018).
2. Manna, K., Sun, Y., Muechler, L., Kübler, J. & Felser, C. Heusler, Weyl and Berry. *Nat. Rev. Mater.* **3**, 244–256 (2018).

3. Hu, J., Xu, S.-Y., Ni, N. & Mao, Z. Transport of topological semimetals. *Annu. Rev. Mater. Res.* **49**, 207–252 (2019).
4. Wang, Z. et al. Time-reversal-breaking Weyl fermions in magnetic Heusler alloys. *Phys. Rev. Lett.* **117**, 236401 (2016).
5. Chang, G. et al. Topological Hopf and Chain link semimetal states and their application to Co_2MnGa. *Phys. Rev. Lett.* **119**, 156401 (2017).
6. Kübler, J. & Felser, C. Weyl points in the ferromagnetic Heusler compound Co_2MnAl. *Europhys. Lett.* **114**, 47005 (2016).
7. Lee, W.-L., Watauchi, S., Miller, V. L., Cava, R. J. & Ong, N. P. Dissipationless anomalous Hall current in the ferromagnetic spinel $CuCr_2Se_{4-x}Br_x$. *Science* **303**, 1647–1649 (2004).
8. Muechler, L. et al. Emerging chiral edge states from the confinement of a magnetic Weyl semimetal in Co3Sn2S2. *Phys. Rev. B* **101**, 115106 (2020).
9. Liu, E. et al. Giant anomalous Hall effect in a ferromagnetic kagome-lattice semimetal. *Nat. Phys.* **14**, 1125–1131 (2018).
10. Belopolski, I. et al. Discovery of topological Weyl fermion lines and drumhead surface states in a room temperature magnet. *Science* **365**, 1278–1281 (2019).
11. Noky, J., Zhang, Y., Gooth, J., Felser, C. & Sun, Y. Giant anomalous Hall and Nernst effect in magnetic cubic Heusler compounds. *npj Comput. Mater.* **6**, 1–8 (2020).
12. Manna, K. et al. From Colossal to Zero: controlling the anomalous Hall effect in magnetic Heusler compounds via Berry curvature design. *Phys. Rev. X* **8**, 041045 (2018).
13. Guin, S. N. et al. Anomalous Nernst effect beyond the magnetization scaling relation in the ferromagnetic Heusler compound Co2MnGa. *NPG Asia Mater.* **11**, 1–9 (2019).
14. Sakai, A. et al. Giant anomalous Nernst effect and quantum-critical scaling in a ferromagnetic semimetal. *Nat. Phys.* **14**, 1119–1124 (2018).
15. Tung, J.-C. & Guo, G.-Y. High spin polarization of the anomalous Hall current in Co-based Heusler compounds. *N. J. Phys.* **15**, 033014 (2013).
16. Lu, Y. M., Cai, J. W., Pan, H. Y. & Sun, L. Ultrasensitive anomalous Hall effect in SiO_2/Fe-Pt/SiO_2 sandwich structure films. *Appl. Phys. Lett.* **100**, 022404 (2012).
17. Iihama, S. et al. Spin-transfer torque induced by the spin anomalous Hall effect. *Nat. Electron.* **1**, 120–123 (2018).
18. Holmes, S. N. & Pepper, M. Magnetic and electrical properties of Co_2MnGa grown on GaAs (001). *Appl. Phys. Lett.* **81**, 1651–1653 (2002).
19. Yu, C., Pechan, M. J., Carr, D. & Palmstrøm, C. J. Ferromagnetic resonance in the stripe domain state: a study in Co_2MnGa (001). *J. Appl. Phys.* **99**, 08J109 (2006).
20. Hassan, S. S. A. et al. The properties and structure relationship of half metallic magnetic materials on GaAs. *IEEE Trans. Magn.* **45**, 4360–4363 (2009).
21. Kudryavtsev, Y. V. et al. Evolution of the magnetic properties of Co_2MnGa Heusler alloy films: From amorphous to ordered films. *Phys. Rev. B* **76**, 024430 (2007).
22. Kolbe, M. et al. Test of band structure calculations for Heusler compounds by spin-resolved photoemission spectroscopy. *Phys. Rev. B* **86**, 024422 (2012).
23. Sato, T. et al. Large negative anisotropic magnetoresistance in Co2MnGa Heusler alloy epitaxial thin films. *Appl. Phys. Lett.* **113**, 112407 (2018).
24. Reichlova, H. et al. Large anomalous Nernst effect in thin films of the Weyl semimetal Co_2MnGa. *Appl. Phys. Lett.* **113**, 212405 (2018).
25. Park, G.-H. et al. Thickness dependence of the anomalous Nernst effect and the Mott relation of Weyl semimetal Co_2MnGa thin films. *Phys. Rev. B* **101**, 060406 (2020).
26. Markou, A. et al. Thickness dependence of the anomalous Hall effect in thin films of the topological semimetal Co_2MnGa. *Phys. Rev. B* **100**, 054422 (2019).
27. Wang, Q., Wen, Z., Kubota, T., Seki, T. & Takanashi, K. Structural-order dependence of anomalous Hall effect in Co_2MnGa topological semimetal thin films. *Appl. Phys. Lett.* **115**, 252401 (2019).
28. Ludbrook, B. M., Ruck, B. J. & Granville, S. Perpendicular magnetic anisotropy in Co_2MnGa and its anomalous Hall effect. *Appl. Phys. Lett.* **110**, 062408 (2017).
29. Mangin, S. et al. Current-induced magnetization reversal in nanopillars with perpendicular anisotropy. *Nat. Mater.* **5**, 210–215 (2006).
30. Sakuraba, Y. et al. Huge spin-polarization of L21-ordered Co_2MnSi epitaxial heusler alloy film. *Jpn. J. Appl. Phys.* **44**, L1100 (2005).
31. Kübler, J. *Theory of Itinerant Electron Magnetism* (Oxford Univ. Press, 2017).
32. Zhu, L. J. & Zhao, J. H. Anomalous resistivity upturn in epitaxial L21-Co_2MnAl films. *Sci. Rep.* **7**, 42931 (2017).
33. Liu, Y. et al. Optically induced magnetization dynamics and variation of damping parameter in epitaxial Co_2MnSi Heusler alloy films. *Phys. Rev. B* **81**, 094402 (2010).
34. Webster, P. J. Magnetic and chemical order in Heusler alloys containing cobalt and manganese. *J. Phys. Chem. Solids* **32**, 1221–1231 (1971).
35. Miyasato, T. et al. Crossover behaviour of the anomalous Hall effect and anomalous Nernst effect in Itinerant Ferromagnets. *Phys. Rev. Lett.* **99**, 086602 (2007).
36. Suzuki, T. et al. Large anomalous Hall effect in a half-Heusler antiferromagnet. *Nat. Phys.* **12**, 1119–1123 (2016).
37. Singha, R., Roy, S., Pariari, A., Satpati, B. & Mandal, P. Magnetotransport properties and giant anomalous Hall angle in the half-Heusler compound TbPtBi. *Phys. Rev. B* **99**, 035110 (2019).
38. Hirschberger, M. et al. The chiral anomaly and thermopower of Weyl fermions in the half-Heusler GdPtBi. *Nat. Mater.* **15**, 1161–1165 (2016).
39. Xiong, J. et al. Evidence for the chiral anomaly in the Dirac semimetal Na3Bi. *Science* **350**, 413–416 (2015).
40. Shama, Gopal,R. K. & Singh, Y. Observation of planar Hall effect in the ferromagnetic Weyl semimetal $Co_3Sn_2S_2$. *J. Magn. Magn. Mater.* **502**, 166547 (2020).
41. Chen, Y.-C. et al. Heteroepitaxy of Co-based Heusler compound/muscovite for flexible spintronics. *ACS Appl. Mater. Interfaces* **11**, 35162–35168 (2019).
42. Tong, S., Zhao, X., Wei, D. & Zhao, J. Low-temperature resistivity anomaly and weak spin disorder in Co_2MnGa epitaxial thin films. *Phys. Rev. B* **101**, 184434 (2020).
43. Nagaosa, N., Sinova, J., Onoda, S., MacDonald, A. H. & Ong, N. P. Anomalous Hall effect. *Rev. Mod. Phys.* **82**, 1539–1592 (2010).
44. Onoda, S., Sugimoto, N. & Nagaosa, N. Intrinsic versus extrinsic anomalous Hall effect in ferromagnets. *Phys. Rev. Lett.* **97**, 126602 (2006).
45. Xiao, D., Chang, M.-C. & Niu, Q. Berry phase effects on electronic properties. *Rev. Mod. Phys.* **82**, 1959–2007 (2010).
46. Sumida, K. et al. Spin-polarized Weyl cones and giant anomalous Nernst effect in ferromagnetic Heusler films. *Commun. Mater.* **1**, 89 (2020).
47. Schindler, C. et al. Effect of uniaxial stress on the electronic band structure of NbP. *Phys. Rev. B* **102**, 035132 (2020).
48. Ayuela, A., Enkovaara, J., Ullakko, K. & Nieminen, R. M. Structural properties of magnetic Heusler alloys. *J. Phys. Condens. Matter* **11**, 2017–2026 (1999).
49. Moritz, J., Rodmacq, B., Auffret, S. & Dieny, B. Extraordinary Hall effect in thin magnetic films and its potential for sensors, memories and magnetic logic applications. *J. Phys. D Appl. Phys.* **41**, 135001 (2008).
50. Vilanova Vidal, E., Stryganyuk, G., Schneider, H., Felser, C. & Jakob, G. Exploring Co_2MnAl Heusler compound for anomalous Hall effect sensors. *Appl. Phys. Lett.* **99**, 132509 (2011).
51. Kim, K. et al. Large anomalous Hall current induced by topological nodal lines in a ferromagnetic van der Waals semimetal. *Nat. Mater.* **17**, 794–799 (2018).
52. Thiyagarajah, N. et al. Giant spontaneous Hall effect in zero-moment Mn2RuxGa. *Appl. Phys. Lett.* **106**, 122402 (2015).
53. Kresse, G. & Furthmüller, J. Efficiency of ab-initio total energy calculations for metals and semiconductors using a plane-wave basis set. *Comput. Mater. Sci.* **6**, 15–50 (1996).
54. Perdew, J. P., Burke, K. & Ernzerhof, M. Generalized gradient approximation made simple. *Phys. Rev. Lett.* **77**, 3865–3868 (1996).
55. Wu, Q., Zhang, S., Song, H.-F., Troyer, M. & Soluyanov, A. A. WannierTools: an open-source software package for novel topological materials. *Comput. Phys. Commun.* **224**, 405–416 (2018).
56. Wang, X., Yates, J. R., Souza, I. & Vanderbilt, D. Ab initio calculation of the anomalous Hall conductivity by Wannier interpolation. *Phys. Rev. B* **74**, 195118 (2006).
57. Mostofi, A. A. et al. wannier90: a tool for obtaining maximally-localised Wannier functions. *Comput. Phys. Commun.* **178**, 685–699 (2008).

ACKNOWLEDGEMENTS

We are grateful to Jérôme Leveneur from GNS science for the AFM measurements and Sarah Spencer from the Robinson Research Institute for EDX. Y.F.Y. and N.M. acknowledge the support from Australian National Computing Infrastructure and Pawsey Supercomputing Centre. The MacDiarmid Institute is supported under the New Zealand Centres of Research Excellence Programme. Y.F.Y. and N.M. are thankful for the funding support from the Australian Research Council (CE170100039).

AUTHOR CONTRIBUTIONS

Y.Z. fabricated and characterized devices with assistance from G.D. and T.B. Y.Z. and S. G. analyzed the data. Y.F.Y. did the theoretical calculations with contributions from N. M. Y.Z. and S.G. wrote the manuscript with contributions from all authors. All authors discussed the results and commented on the manuscript. The study was performed under the supervision of S.G.

COMPETING INTERESTS

The authors declare no competing interests.

ADDITIONAL INFORMATION

Supplementary information The online version contains supplementary material available at https://doi.org/10.1038/s41535-021-00315-8.

Correspondence and requests for materials should be addressed to N.V.M. or S.G.

Reprints and permission information is available at http://www.nature.com/reprints

Publisher's note Springer Nature remains neutral with regard to jurisdictional claims in published maps and institutional affiliations.